

The Origin of the Charge Ordering and Its Relevance to Superconductivity in θ -(BEDT-TTF) $_2$ X: The Effect of the Fermi Surface Nesting and the Distant Electron-Electron Interactions

Kazuhiko Kuroki

Department of Applied Physics and Chemistry, The University of Electro-Communications, Chofu, Tokyo 182-8585, Japan

The origin of the charge ordering in organic compounds θ -(BEDT-TTF) $_2$ X ($X = MM'(\text{SCN})_4$, $M = \text{Ti, Rb, Co}$, $M' = \text{Cs, Zn}$) is studied using an extended Hubbard model. Calculating the charge susceptibility within random phase approximation (RPA), we find that the $(3 \times 3) \sim (3 \times 4)$ charge ordering observed at relatively high temperatures can be considered as a consequence of a cooperation between the Fermi surface nesting, controlled by the hopping integral in the c direction, and the electron-electron interactions, where the distant (next nearest neighbor) interactions that have not been taken into account in most of the previous studies play an important role. Mean field analysis at $T = 0$ also supports the RPA results, and further shows that in the 3×3 charge ordered state, some portions of the Fermi surface remain ungapped and are nested with a nesting vector close to the modulation wave vector of the horizontal stripe ordering observed at low temperatures in $X = MM'(\text{SCN})_4$. We further study the possibility of superconductivity by taking into account the distant off-site repulsions and the band structure corresponding to $X = \text{I}_3$, in which superconductivity is experimentally observed. We find that there is a close competition between d_{xy} -wave-like singlet pairing and p_{x+2y} -wave-like triplet pairing due to a cooperation between the charge and the spin fluctuations. The present analysis provides a possible unified understanding of the experimental phase diagram of the θ -(BEDT-TTF) $_2$ X family, ranging from a charge ordered insulator to a superconductor.

KEYWORDS: θ -(BEDT-TTF) $_2$ X, charge ordering and fluctuations, electron-electron interactions, Fermi surface, pairing symmetry

1. Introduction

θ -(BEDT-TTF) $_2$ X is one of the most interesting families of organic compounds, ranging from charge ordered insulators such as $X = \text{RbZn}(\text{SCN})_4$ to a superconductor $X = \text{I}_3$.^{1,2} The anion X controls the angle between the BEDT-TTF molecules, which in turn determines the band structure. A further fascination for this series of compounds has arisen by a recent observation of a giant nonlinear transport in $X = \text{CsM}'(\text{SCN})_4$ ($M' = \text{Co, Zn}$), which makes the material work as an organic thyristor.^{3,4} There, it has been pointed out that the coexistence of two kinds of short range charge ordering with modulation wave vectors $(q_a, q_b, q_c) = (\frac{2}{3}, k, \frac{1}{3})$ and $(0, k, \frac{1}{2})$ (in units of the reciprocal lattice primitive vectors in a, b, c directions; a and c directions are shown in Fig.1) plays an important role in this phenomenon. The $(\frac{2}{3}, k, \frac{1}{3})$ modulation corresponds to a 3×3 ordering with respect to the a - c unit cell shown in Fig.1, while a charge modulation with $(0, k, \frac{1}{2})$ is often referred to as the horizontal stripe ordering (Fig.2). At high temperatures, a diffuse X-ray spot is observed at $(\frac{2}{3}, k, \frac{1}{3})$,^{5,6} while the $(0, k, \frac{1}{2})$ structure develops as temperature is lowered, and the system becomes more insulating. When the electric field is applied, the $(0, k, \frac{1}{2})$ horizontal stripe ordering is degraded, resulting in a recovery of the metallic behavior and thus the nonlinear transport. Related to this is an observation of lattice modulation with a wave vector $(\frac{2}{3}, k, 0.29 \sim \frac{1}{3})$ in $X = \text{CsCo}(\text{SCN})_4$ under pressure of 10kbar, which has been attributed to a pressure induced $2k_F$ charge den-

sity wave (CDW) because the modulation wave vector coincides with the nesting vector of the Fermi surface.⁶

In $X = \text{RbM}'(\text{SCN})_4$ ($M' = \text{Co, Zn}$) also, two kinds of charge ordering are involved. At high temperatures in the metallic phase, diffuse X-ray spots are observed at $(\frac{2}{3}, k, \frac{1}{4})$ and $(\frac{1}{3}, k, \frac{3}{4})$, which suggests the presence of short range 3×4 charge ordering.^{7,8} Some anomalies are also observed in the NMR experiments in the similar temperature range.^{9,10} At around 200K, the system undergoes a metal-insulator transition, accompanied by a structural phase transition into the so-called θ_d phase,¹¹ in which the unit cell is doubled in the c direction.^{2,7-10,12-14} In the θ_d phase, X-ray diffraction measurements have revealed that a long range horizontal stripe charge ordering with the modulation wave vector $(0, 0, \frac{1}{2})$ takes place.^{1,2,7,8}

Theoretically, the origin of these charge orderings has been an issue of great interest. Although some orderings are accompanied by structural phase transition or lattice modulation such as the horizontal stripe ordering in $X = \text{RbM}'(\text{SCN})_4$ and the $(\frac{2}{3}, k, 0.29 \sim \frac{1}{3})$ ordering ($2k_F$ CDW) in $X = \text{CsM}'(\text{SCN})_4$ under pressure, such a lattice modulation is not observed when the $(0, k, \frac{1}{2})$ (horizontal stripe) short range order develops in $X = \text{CsM}'(\text{SCN})_4$, nor when $3 \times (3 \sim 4)$ ordering occurs in $X = MM'(\text{SCN})_4$ at ambient pressure. Therefore, it is reasonable to assume that the electronic degrees of freedom takes the initiative in these charge orderings, and in some cases the lattice modulation occurs as a *con-*

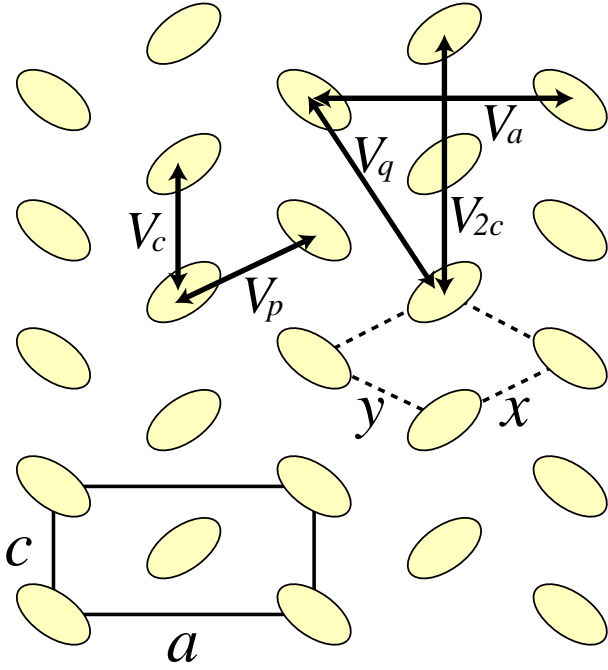


Fig. 1. The lattice structure of the cation layer of θ -(BEDT-TTF) $_2$ X. V_p , V_c are the nearest neighbor interactions, while V_a , V_q , V_{2c} are the next nearest neighbor interactions. The a - c unit cell is the usual unit cell, while we can use the x - y unit cell to unfold the BZ.

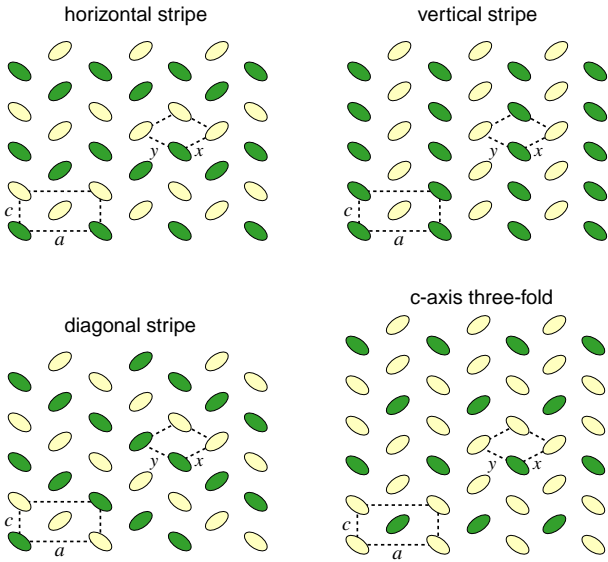


Fig. 2. (Color online) Horizontal stripe, vertical stripe, diagonal stripe, and c -axis three-fold charge orderings are shown. The green (or dark) molecules are the charge rich ones.

sequence of the electronic charge modulation. In understanding the origin of the charge ordering in θ -(BEDT-TTF) $_2$ X from a purely electronic point of view, an important progress was made by Seo, who included the nearest neighbor off-site repulsions V_p and V_c in the model Hamiltonian (see Fig.1).¹¹ There have also been studies on a model that neglects V_c ,^{15,16} but an estimation by Mori¹⁷ shows that $V_p \sim V_c$ for the θ -(BEDT-TTF) compounds. In ref.11, the energy of various types of charge

ordering patterns, such as horizontal, vertical, and diagonal stripes (Fig.2), was calculated within the mean field approximation. There, it was found, however, that the horizontal stripe charge ordering is not stabilized for the θ -phase lattice structure, while it is stabilized in a certain parameter regime in the θ_d lattice structure, which has a two-fold modulation in the c -axis direction. Thus, within this analysis, the lattice modulation seems to be the cause, not a consequence, of the electronic charge stripe formation. Exact diagonalization studies on these stripe orders have also been performed,^{18,19} but in the mean while, an analysis by Mori in the static limit revealed a possibility of non-stripe charge ordering shown in Fig.2,¹⁷ which has a three-fold periodicity in the c -axis direction. We will call this the “ c -axis three-fold” charge ordering in the present paper. Later on, Kaneko and Ogata extended Seo’s mean field study to take into account the possibility of this c -axis three-fold ordering,²⁰ where they found that this ordering does have a lower energy than the vertical, diagonal, and horizontal stripes when $V_p \sim V_c$. In these studies, a possible relation between the c -axis three-fold ordering and the diffuse X-ray spots observed at $(\frac{2}{3}, k, \frac{1}{3} \sim \frac{1}{4})$ was suggested. A variational Monte Carlo study by Watanabe and Ogata found a subtle competition between the c -axis three-fold ordered state and the diagonal or vertical stripe states,²¹ but quite recently, Hotta *et al.* used exact diagonalization for a spinless half-filled model, which can be considered as an effective model of the θ -type compounds in the large on-site U limit, and showed the presence of c -axis three-fold charge correlation for $V_p \sim V_c$.²²

In the present study, we will further confirm that the c -axis three-fold charge correlation is strong when $V_p \sim V_c$. Moreover, we point out that while the c -axis three-fold charge ordering is uniform in the a -axis direction, the diffuse X-ray spots are observed at $(\frac{2}{3}, k, \frac{1}{3} \sim \frac{1}{4})$, which corresponds to orderings with a three-fold periodicity in the a -axis direction. We stress here that the common (and thus probably the most essential) feature in the high temperature charge ordering is the three-fold periodicity in the a -axis direction ($q_a = \frac{2}{3}$), while the periodicity in the c -axis direction is sensitive to the anions and/or the pressure. Thus, we conclude that neither the low temperature horizontal stripe nor the high temperature $3 \times (3 \sim 4)$ charge orderings can be understood within purely electronic models that consider only V_p and V_c (with $V_p \sim V_c$) as off-site repulsions. We argue that the consideration of more distant (next nearest neighbor) electron-electron interactions is crucial, and propose that the cooperation between the Fermi surface nesting and the electron-electron interactions including those distant ones is the origin of the charge orderings.

Another aim of the present study is to investigate the origin of superconductivity in $X = I_3$.²³ Since this material sits in the vicinity of the (nearly) charge ordered materials in the experimental phase diagram,² it is interesting to investigate whether the charge fluctuations can give rise to the occurrence of superconductivity. The mechanism of superconductivity in θ -type compounds has been studied theoretically in the past,^{21,24,25} but the distant interactions beyond V_p and V_c that are

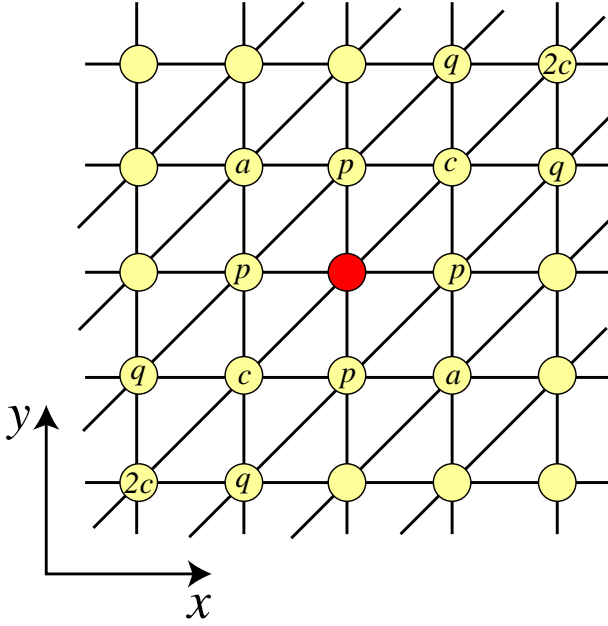


Fig. 3. (Color online) The effective lattice structure using the x - y unit cell. We specify the hoppings and the interactions by c , p , a , q , $2c$, which specify the position relative to the center (red) site.

necessary to understand the charge ordering pattern for $X = MM'(\text{SCN})_4$ were not included there. Since it is natural to assume that the range of the off-site interaction does not change drastically with the change of the anion, we investigate the possibility of superconductivity in the vicinity of the charge ordering phase in a model that takes into account the distant interactions and the band structure of $X = \text{I}_3$.

2. Formulation

2.1 Model

In the lattice structure of θ -(BEDT-TTF) $_2$ X shown in Fig.1, the direction of the molecules alternates along the a axis resulting in the rectangular a - c unit cell, but this alternation is irrelevant as far as the hopping integrals in the tight binding model are concerned. Therefore, we can take a unit cell (x - y) which is half the size of the usual unit cell, thereby obtaining the effective lattice structure shown in Fig.3. The corresponding Brillouin zone (BZ) becomes unfolded, and the relation between the unfolded and the folded BZ is shown in Fig.4. Here, the wave vectors are denoted in units of the reciprocal lattice primitive vectors, and the subscripts uf or f indicate whether the reciprocal vectors are those of the unfolded or the folded BZ. The points $(\frac{2}{3}, k, \frac{1}{3} \sim \frac{1}{4})_f$ at which the diffuse X-ray spots are observed in the high temperature regime of $X = MM'(\text{SCN})_4$ fall on the diagonal line noted as $k_a = \frac{2}{3}$, which is a line that satisfies $k_x - k_y = \frac{2}{3}$ in the unfolded BZ. It can be clearly seen that these positions are different from the modulation wave vector of the c -axis three-fold ordering, $(0, \frac{2}{3})_f = (\frac{1}{3}, \frac{1}{3})_{uf}$.

We consider an extended Hubbard model on the lattice shown in Fig.3, where the Hamiltonian is given in the

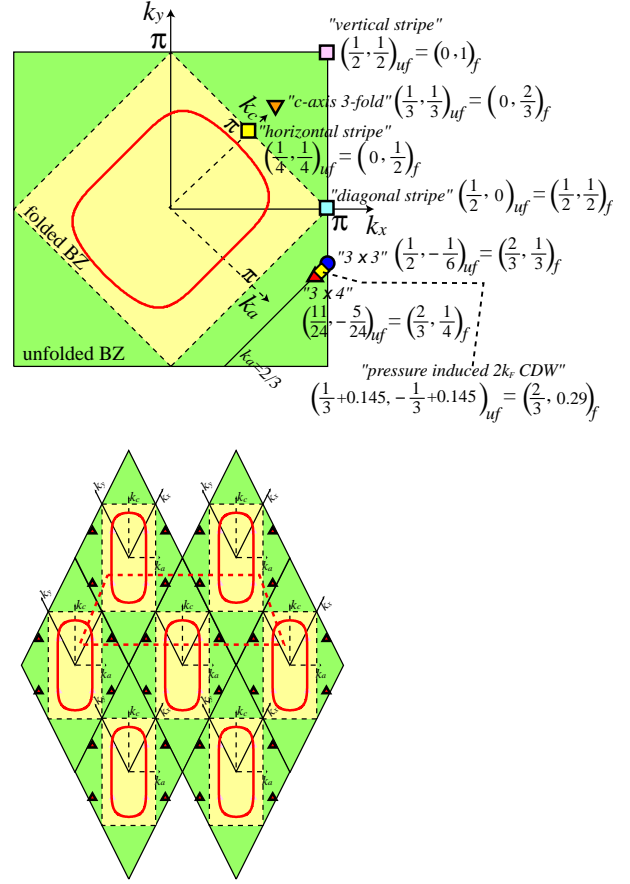


Fig. 4. (Color online) Upper panel: The relation between the folded and the unfolded BZ is shown. Modulation wave vectors corresponding to various orderings are shown. The wave vectors are presented in units of the reciprocal lattice primitive vectors. The red line shows the Fermi surface for $t_c = -0.3$. Lower panel: The BZ in the upper panel is squeezed in the $k_x = -k_y$ direction, and then placed repeatedly. The trapezoid area surrounded by the red dashed line corresponds to the area at which the X-ray diffuse rods are observed in Fig.4(a) of ref.7.

form

$$H = \sum_{\langle i,j \rangle, \sigma} t_{ij} c_{i\sigma}^\dagger c_{j\sigma} + U \sum_i n_{i\uparrow} n_{i\downarrow} + \sum_{\langle i,j \rangle} V_{ij} n_i n_j, \quad (1)$$

where $c_{i\sigma}^\dagger$ creates an electron with spin $\sigma = \uparrow, \downarrow$ at site i , and $n_{i\sigma} = c_{i\sigma}^\dagger c_{i\sigma}$. The band filling, the average number of electrons per site (molecule), is fixed at $n = 1.5$ in accord with the actual material. In Fig.3, the letters p , c , a , \dots denote the relative positions with respect to the red site in the center, and we use these letters to specify the range of the hopping integrals and the off-site repulsive interactions. As for the kinetic energy terms, we consider hoppings t_p and t_c , where $t_p (\simeq 0.1\text{eV})$ is taken as the unit of energy. U is the on-site repulsive interaction. As for the off-site repulsions, we consider, in addition to V_p and V_c (nearest neighbor interactions) that are usually taken into account, more distant interactions V_a , V_q , and V_{2c} (next nearest neighbor interactions, see also Fig.1). Consideration of these interactions is supported by Mori's estimation showing that these distant interactions are not so small compared to V_p and V_c .¹⁷ Also, there is a recent trans-

port experiment which indicates that the repulsive interaction in θ -(BEDT-TTF)₂MZn(SCN)₄ ($M = \text{Cs, Rb}$) is long ranged.²⁶ In fact, the presence of such a distant interaction has also been pointed out theoretically for quasi-one-dimensional organic compounds (TMTSF)₂X in the context of coexisting $2k_F$ spin and $2k_F$ charge density waves^{27–29} and spin triplet pairing superconductivity.^{29–34} So there is a possibility that long ranged nature of the electron-electron interaction may be common in these organic materials. Since the values of the electron-electron repulsions have not so far been strictly estimated from, e.g., first principles calculations, here we vary them as parameters and investigate whether the experimentally observed charge orderings can be understood within a realistic parameter regime, where we take V_a, V_q, V_{2c} to be smaller than $\sim V_c/2$, and $V_c \simeq V_p$ to be smaller than $\sim U/2$.

2.2 Random Phase Approximation

In this subsection, we describe the random phase approximation (RPA) adopted in the present study. Within RPA,^{25, 35, 36} the spin and charge susceptibilities, χ_s and χ_c , respectively, are given as

$$\begin{aligned}\chi_s(\mathbf{q}) &= \frac{\chi_0(\mathbf{q})}{1 - U\chi_0(\mathbf{q})} \\ \chi_c(\mathbf{q}) &= \frac{\chi_0(\mathbf{q})}{1 + (U + 2V(\mathbf{q}))\chi_0(\mathbf{q})}.\end{aligned}\quad (2)$$

Here χ_0 is the bare susceptibility given by

$$\chi_0(\mathbf{q}) = \frac{1}{N} \sum_{\mathbf{p}} \frac{f(\epsilon_{\mathbf{p} + \mathbf{q}}) - f(\epsilon_{\mathbf{p}})}{\epsilon_{\mathbf{p}} - \epsilon_{\mathbf{p} + \mathbf{q}}}\quad (3)$$

with $\epsilon_{\mathbf{k}}$ being the band dispersion given as

$$\epsilon_{\mathbf{k}} = 2t_p[\cos(k_x) + \cos(k_y)] + 2t_c \cos(k_x + k_y)\quad (4)$$

and $f(\epsilon_{\mathbf{p}}) = 1/(\exp(\epsilon_{\mathbf{p}} - \mu)/T) + 1$ is the Fermi distribution function. When the nesting of the Fermi surface is good, $\chi_0(\mathbf{q})$ is maximized at the nesting vector. $V(\mathbf{q})$ is the Fourier transform of the off-site repulsions, given as

$$\begin{aligned}V(\mathbf{q}) &= 2V_p[\cos(q_x) + \cos(q_y)] \\ &+ 2V_c \cos(q_x + q_y) + 2V_a \cos(q_x - q_y) \\ &+ 2V_q[\cos(2q_x + q_y) + \cos(q_x + 2q_y)] \\ &+ 2V_{2c} \cos(2q_x + 2q_y)\end{aligned}\quad (5)$$

To discuss superconductivity, the effective pairing interactions for the singlet and triplet channels due to spin and charge fluctuations are given as

$$\begin{aligned}V_{singlet}^{pair}(\mathbf{q}) &= U + V(\mathbf{q}) + \frac{3}{2}U^2\chi_s(\mathbf{q}) \\ &- \frac{1}{2}(U + 2V(\mathbf{q}))^2\chi_c(\mathbf{q})\end{aligned}\quad (6)$$

$$\begin{aligned}V_{triplet}^{pair}(\mathbf{q}) &= V(\mathbf{q}) - \frac{1}{2}U^2\chi_s(\mathbf{q}) \\ &- \frac{1}{2}(U + 2V(\mathbf{q}))^2\chi_c(\mathbf{q}).\end{aligned}\quad (7)$$

To obtain the superconducting transition temperature T_c , we solve the linearized gap equation within the weak-coupling theory,

$$\lambda\Delta(\mathbf{k}) = -\frac{1}{N} \sum_{\mathbf{k}'} V^{pair}(\mathbf{k} - \mathbf{k}') \frac{\tanh(\beta\epsilon_{\mathbf{k}'}/2)}{2\epsilon_{\mathbf{k}'}} \Delta(\mathbf{k}').\quad (8)$$

The eigenfunction Δ of this eigenvalue equation is the gap function. The transition temperature T_c is determined as the temperature where the largest eigenvalue λ reaches unity. In the actual numerical calculations, we take up to $N = 256 \times 256$ k -point meshes.

2.3 Mean Field Approximation

In the mean field approximation, we approximate the interaction terms $n_{i\sigma}n_{j\sigma'}$ by $n_{i\sigma}\langle n_{j\sigma'} \rangle + \langle n_{i\sigma} \rangle n_{j\sigma'}$. We assume an electron density modulation with a modulation vector $(\frac{1}{2}, -\frac{1}{6})_{uf}$ (two-fold periodicity in the x direction and six-fold periodicity in the y direction), resulting in a unit cell that contains six sites (see the inset of Fig.12 in section 3.2). This corresponds to the 3×3 ordering in the original lattice structure because $(\frac{2}{3}, \frac{1}{3})_f = (\frac{1}{2}, -\frac{1}{6})_{uf}$. Here we neglect the spin ordering for simplicity, i.e., $\langle n_{i\uparrow} \rangle = \langle n_{i\downarrow} \rangle$, because (i) the ordering of the spins, if any, should take place in accord with the nesting vector of the Fermi surface, and therefore incommensurate and difficult to deal with, and (ii) the main aim of the mean field analysis is just to reinforce the RPA results and also to obtain the Fermi surfaces in the charge ordered state. We do not compare the total energy between different ordering states to pin down the ground state because (i) we do not consider the spin ordering properly and (ii) there could be a number of candidates for the ground state including incommensurate states. We obtain the band structure in the presence of the $(\frac{1}{2}, -\frac{1}{6})_{uf}$ ordering, and then calculate $\langle n_{i\sigma} \rangle$ at $T = 0$, which is substituted back into the mean field Hamiltonian, and the band structure is calculated again. These procedures are repeated until all $\langle n_{i\sigma} \rangle$ are self-consistently determined. We define

$$\Delta n_{\max} = n_{\max\uparrow} - \langle n_{\uparrow} \rangle,\quad (9)$$

where $n_{\max\uparrow}$ is the largest up(=down) spin electron density among the six sites and $\langle n_{\uparrow} \rangle$ is the average up spin electron density, 0.75 in the present case. In the actual numerical calculations, we take up to 200×200 unit cells.

3. Charge fluctuations and ordering

3.1 Random Phase Approximation

First we consider the case when $t_c = 0$ and $V_a = V_q = V_{2c} = 0$. In Fig.5, we show the RPA charge susceptibility for $U = 3$ and $V_c = 1.5$. In the case of $V_p = 1.5$, there is a peak at $(\frac{1}{3}, \frac{1}{3})_{uf}$, which corresponds to $(0, \frac{2}{3})_f$ in the original BZ, namely, the modulation wave vector of the c -axis three-fold ordering. This is due to a peak in $-V(\mathbf{q})$ at $\mathbf{q} = (\frac{1}{3}, \frac{1}{3})_{uf}$ as shown in Fig.5. Namely, although $\chi_0(\mathbf{q})$ is maximized around $(0, \pm\frac{1}{6})_{uf}$ and $(\pm\frac{1}{6}, 0)_{uf}$, the effect of $-V(\mathbf{q})$ dominates in the denominator of the RPA formula of the charge susceptibility eq.(2), thereby minimizing the denominator and maximizing $\chi_c(\mathbf{q})$ at $(\frac{1}{3}, \frac{1}{3})_{uf}$. For V_p slightly smaller than V_c , which is more realistic for θ -(BEDT-TTF) compounds,¹⁷ the peak at $(\frac{1}{3}, \frac{1}{3})_{uf}$ still

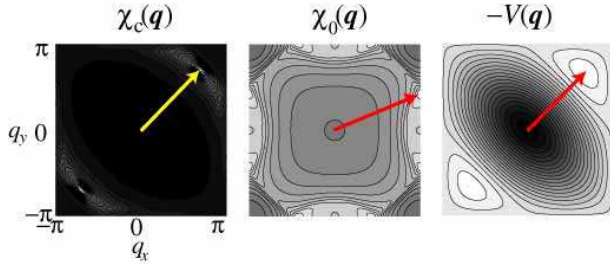


Fig. 5. (Color online) Contour plots of the RPA result of the charge susceptibility χ_c , the bare susceptibility χ_0 , and the Fourier transform of the off-site interactions $-V(q)$ are shown. $t_c = 0$, $U = 3$, $V_p = V_c = 1.5$, $V_a = V_q = V_{2c} = 0$, $T = 0.05$, all in units of t_p . The arrows represent the wave vector at which each function takes its maximum.

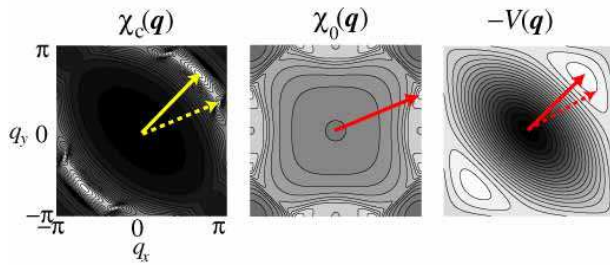


Fig. 6. (Color online) Plots similar to Fig. 5 except that $V_p = 1.3$. Other parameters are the same: $t_c = 0$, $U = 3$, $V_c = 1.5$, $V_a = V_q = V_{2c} = 0$. In χ_c , the dashed arrow shows the wave vector at which a subdominant peak exists. The dashed arrow in $-V(q)$ indicates that the wave vectors at which $-V(q)$ takes large values extend toward $(\frac{1}{2}, 0)_{uf}$ compared to the case shown in Fig. 5

remains (Fig. 6), but there also appears a subdominant peak around a wave vector somewhat close to $(\frac{1}{2}, 0)_{uf}$, i.e., the modulation vector of the diagonal stripe. The origin of this second peak becomes more clear if we further introduce a finite $t_c = -0.3$, which roughly corresponds to the case of $X = \text{RbM}'(\text{SCN})_4$ ($M' = \text{Zn, Co}$) or $X = \text{CsCo}(\text{SCN})_4$ under pressure.⁶ In this case, the nesting of the Fermi surface (see Fig. 4) becomes good around $(\frac{2}{3}, \frac{1}{4})_f = (\frac{11}{24}, -\frac{5}{24})_{uf}$, as can be seen from the bare susceptibility χ_0 shown in Fig. 7. Now the peak near $(\frac{1}{2}, 0)_{uf}$ has about the same height as that at $(\frac{1}{3}, \frac{1}{3})_{uf}$, which is due to a combination of $\chi_0(q)$ that has large values extending from the nesting position toward $(\frac{1}{2}, 0)_{uf}$, and $-V(q)$ in which large values extend to wave vectors closer to $(\frac{1}{2}, 0)_{uf}$ when $V_p < V_c$.

Thus, in all of the cases studied above, the peak position of the charge susceptibility disagree with the experimental observations. We have looked into various other cases with $V_c \sim V_p$ and $V_a = V_q = V_{2c} = 0$, where we always found that the charge susceptibility does not have a peak at $(\frac{1}{2}, -\frac{1}{6})_{uf} \sim (\frac{11}{24}, -\frac{5}{24})_{uf} = (\frac{2}{3}, \frac{1}{3} \sim \frac{1}{4})_f$, corresponding to $3 \times (3 \sim 4)$ modulation, nor at $(\frac{1}{4}, \frac{1}{4})_{uf} = (0, \frac{1}{2})_f$, which corresponds to the horizontal stripe modulation.

Thus the model that considers only U , V_p , and V_c as electron-electron repulsions fails to explain the experi-

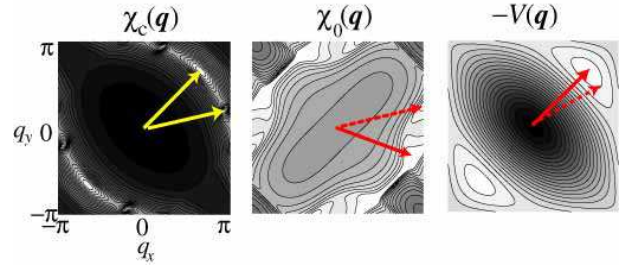


Fig. 7. (Color online) Plots similar to Fig. 6 except that $t_c = -0.3$. Other parameters are the same: $U = 3$, $V_p = 1.3$, $V_c = 1.5$, $V_a = V_q = V_{2c} = 0$. The dashed arrow in $\chi_0(q)$ indicates that the wave vectors at which $\chi_0(q)$ takes large values extend toward the end point of this arrow.

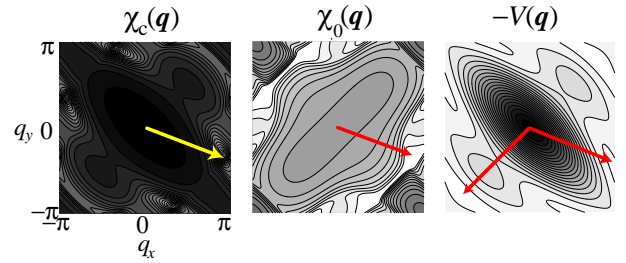


Fig. 8. (Color online) Plots similar to Fig. 7 except that $V_a = 0.3$, $V_q = 0.5$, $V_{2c} = 0.7$. Other parameters are the same: $t_c = -0.3$, $U = 3$, $V_p = 1.3$, $V_c = 1.5$, $T = 0.05$.

mentally observed charge orderings. Since we believe that the electronic degrees of freedom is responsible for these orderings, we now turn on the distant interactions V_a , V_q , V_{2c} . In Figs. 8 and 9(a), we show the charge susceptibility for $U = 3$ and $U = 4$ with $t_c = -0.3$, maintaining the ratios of the off-site repulsions to U roughly the same. In both cases we find a peak near the positions at which the diffuse X-ray spots are observed in the metallic phase of $X = \text{MM}'(\text{SCN})_4$. This is due to the fact that in these cases, $-V(q)$ is now broadly maximized in a region that includes the nesting vector position, as shown in Figs. 8 and 9(a). Therefore, the denominator in eq. (2) is now minimized at a position close to the nesting vector, resulting in the charge susceptibility peak position that nearly coincides with the diffuse X-ray spot positions.

In Fig. 9(b), we show the result for $t_c = -0.05$ with other parameters being the same with (a). This choice of t_c corresponds to $X = \text{CsM}'(\text{SCN})_4$ at ambient pressure.⁶ In this case, the peak position of the charge susceptibility moves toward the unfolded BZ edge, i.e., closer to $(\frac{1}{2}, -\frac{1}{6})_{uf} = (\frac{2}{3}, \frac{1}{3})_f$, as compared to the case with $t_c = -0.3$. This is because the nesting vector of the Fermi surface is closer to $(\frac{2}{3}, \frac{1}{3})_f$ as can be seen in the figure of χ_0 . This tendency is again consistent with the experimental fact that diffused X-ray spots at high temperatures are observed at $q_c = \frac{1}{3}$ in $X = \text{CsM}'(\text{SCN})_4$ at ambient pressure, while they are at $\frac{1}{4} \leq q_c \leq \frac{1}{3}$ in $X = \text{CsM}'(\text{SCN})_4$ under pressure and in $X = \text{RbM}'(\text{SCN})_4$.

Here we have presented the charge susceptibility for certain choices of interaction values, but we have also

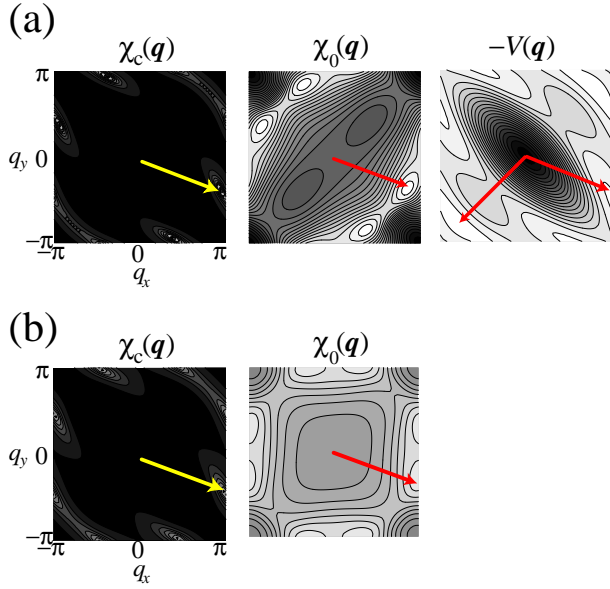


Fig. 9. (Color online) (a) Plots similar to Fig.8 with $t_c = -0.3$, $U = 4$, $V_p = 1.8$, $V_c = 2.0$, $V_a = 0.4$, $V_q = 0.7$, $V_{2c} = 1.1$, $T = 0.25$. (b) Plots similar to (a) except that $t_c = -0.05$. $V(\mathbf{q})$ is the same with that shown in (a).

investigated cases with other sets of parameter values and found similar peak positions of the charge susceptibility within a certain parameter regime. In Fig.10, we show the values of the distant interactions for which the charge susceptibility has a peak close to the the diffuse X-ray spot positions, where “close” means $(q_x, q_y)_{uf}$ within the range of $0.45 \leq q_x \leq \frac{1}{2}$ and $-\frac{1}{4} \leq q_y \leq -\frac{1}{6}$. As seen from this figure, we may say that good agreement with the experimental observation, as far as the peak *position* of the charge susceptibility is concerned, is obtained when $V_a + V_q$ is roughly constant for a given V_{2c} . The peak *height* (the strength of the charge fluctuations) on the other hand becomes higher for larger V_a and smaller V_q , which is because $-V(\mathbf{q})$ around $\mathbf{q} = (\frac{1}{2}, -\frac{1}{6})_{uf} \sim (\frac{11}{24}, -\frac{5}{24})_{uf}$ is larger in this case, so that the cooperation between the off-site repulsions and the Fermi surface nesting becomes more effective.

Thus, in our present view, the $3 \times (3 \sim 4)$ charge ordering found in the high temperature metallic phase of $X = MM'(\text{SCN})_4$ occurs due to a cooperation between the Fermi surface nesting and the effect of the off-site interactions including not only V_c and V_p but also V_a , V_q , V_{2c} . Note that the term “charge ordering” is usually used as a real space ordering of charges that is caused by the repulsive electron-electron interactions (regardless of the shape of the Fermi surface), while a “charge density wave” is caused mainly by the nesting of the Fermi surface. Since the Fermi surface nesting and the electron repulsion cooperate in the present view, the charge ordering in the metallic phase of $X = MM'(\text{SCN})_4$ can be considered as a mixture of these two concepts. In this sense, the $3 \times (3 \sim 4)$ charge ordering is conceptually different from the c -axis three-fold charge ordering in that the latter has nothing to do with the Fermi surface nesting. We believe that chances of the diffuse X-ray spots

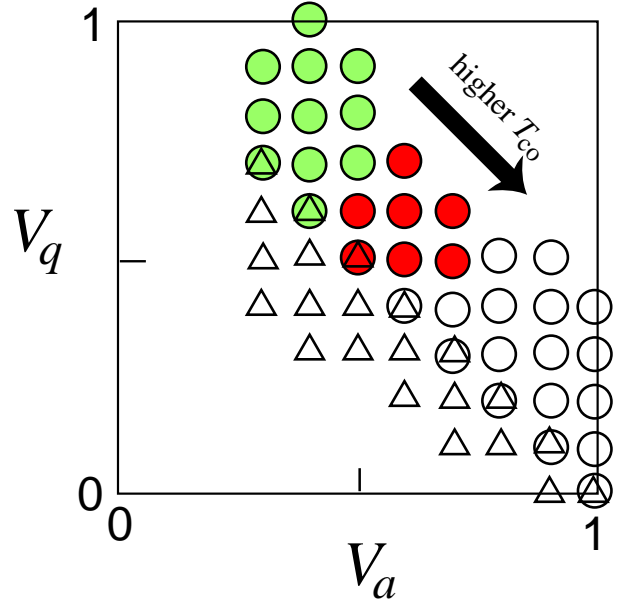


Fig. 10. (Color online) Marked by circles ($V_{2c} = 1.1$) or by triangles ($V_{2c} = 0.7$) are the values of (V_a, V_q) for which the charge susceptibility peak exists near the diffuse X-ray spot positions in the metallic phase (see text) for $t_c = -0.3$, $U = 4$, $V_p = 1.8$, and $V_c = 2.0$. The red (or dark) [green (or light)] circles are the values of (V_a, V_q) for which triplet [singlet] pairing superconductivity dominates for $t_c = +0.2$ (see section3.1). For (V_a, V_q) with uncolored (open) circles, charge ordering occurs above $T = 0.2$ for $t_c = +0.2$.

accidentally coinciding with the nesting vector are very slim, and that the Fermi surface nesting must have something to do with the $3 \times (3 \sim 4)$ charge ordering, while on the other hand, we do believe that the electronic degrees of freedom, not the lattice, is the origin of this ordering.

Now, to further show that the value of t_c is important for the charge fluctuations and ordering, we show in Fig.11 the charge ordering temperature T_{co} , defined as the temperature at which the RPA charge susceptibility diverges at a certain \mathbf{q} , as a function of t_c . T_{co} decreases with the increase of t_c (from $t_c < 0$ to $t_c > 0$), and sharply drops for $t_c > 0$. In fact, the increase of t_c induces several effects. First, the nesting of the Fermi surface is degraded (compare Fermi surfaces in Fig.4 ($t_c < 0$) and Fig.15 ($t_c > 0$)), secondly, the nesting vector deviates from the region where $-V(\mathbf{q})$ is maximized, and thirdly, the density of states near the Fermi level becomes smaller.³⁷ These factors cooperate to work destructively against charge ordering.

This t_c dependence of T_{co} is reminiscent of the phase diagram of the θ -(BEDT-TTF) family obtained by Mori *et al.*,² where charge ordering takes place for compounds having large negative t_c such as $X = \text{Rb}M'(\text{SCN})_4$, while it does not for compounds having small or positive t_c like $X = \text{I}_3$. However, note that in Fig.11, the charge ordering takes place at T_{co} with a modulation wave vector close to the nesting vector of the Fermi surface (around $(\frac{2}{3}, \frac{1}{3} \sim \frac{1}{4})_f$ for $t_c < 0$), while the charge ordering temperature in the experimental phase diagram is those for the $(0, k, \frac{1}{2})_f$ ordering, i.e., the horizontal stripe state. In fact, although we have succeeded in understanding

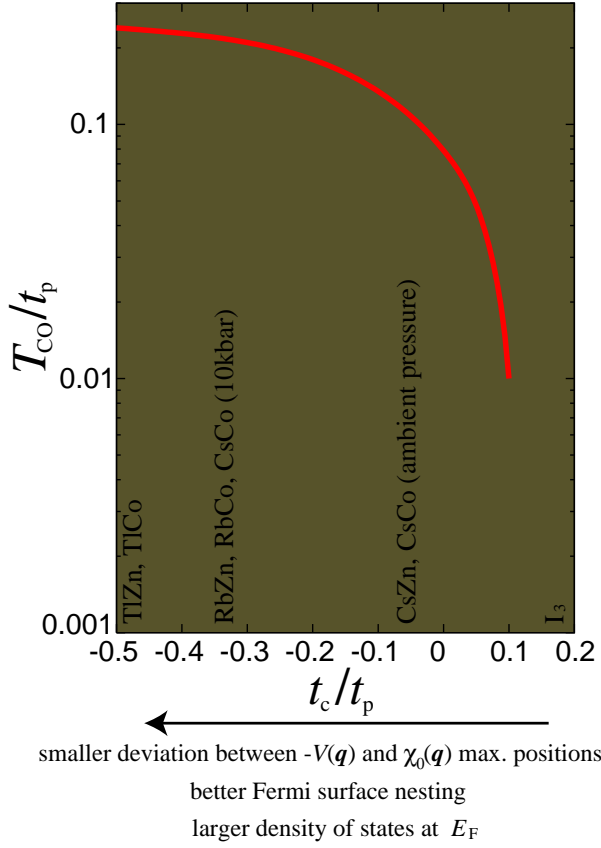


Fig. 11. (Color online) T_{Co} is plotted as a function of t_c for $U = 4$, $V_p = 1.8$, $V_c = 2.0$, $V_a = 0.4$, $V_q = 0.7$, and $V_{2c} = 1.1$. $t_p \simeq 0.1eV \sim 1000K$ is taken as the unit of temperature. The values of t_c/t_p for $X = MM'(SCN)_4$ has been taken from table II in ref.6. As for $X = I_3$, the value of t_p is taken from ref.2 while that of t_c is from ref.42.

the high temperature $3 \times (3 \sim 4)$ ordering, the horizontal $(0, k, \frac{1}{2})_f$ ordering remains to be explained. Namely, there is no trace of enhanced charge fluctuations around $(\frac{1}{4}, \frac{1}{4})_{uf} = (0, \frac{1}{2})_f$ in the charge susceptibility shown in Figs.8 and 9. We will come back to this point in the latter part of the next section.

3.2 Mean Field Approximation

We now move on to the mean field analysis at $T = 0$. As mentioned in section 2.3, we assume 3×3 ordering shown in Fig.12. The actual calculation is done for the ordering shown in the inset. We take values of the interactions to be slightly larger than those adopted in the RPA calculation, $U = 5$, $V_p = 2.2$, $V_c = 2.5$, $(V_a, V_q, V_{2c}) = \alpha(0.5, 0.8, 1.2)$, thereby roughly maintaining the ratios of the off-site repulsions to U when $\alpha = 1$.³⁸ α is a parameter introduced so as to investigate the effect of the distant interactions in a continuous manner.

In Fig.13(a), we show Δn_{max} defined by eq.(9) as a function of t_c for $\alpha = 1$. Here again, we find a similar tendency as found in the RPA calculation, namely, large negative t_c induces the 3×3 charge ordering. In Fig.13(b), we plot Δn_{max} as functions of α for various values of t_c . Here also, we find a tendency that the distant interactions induce the 3×3 charge ordering. For $t_c = -0.3$, we find a finite Δn_{max} solution even for $\alpha = 0$, which is

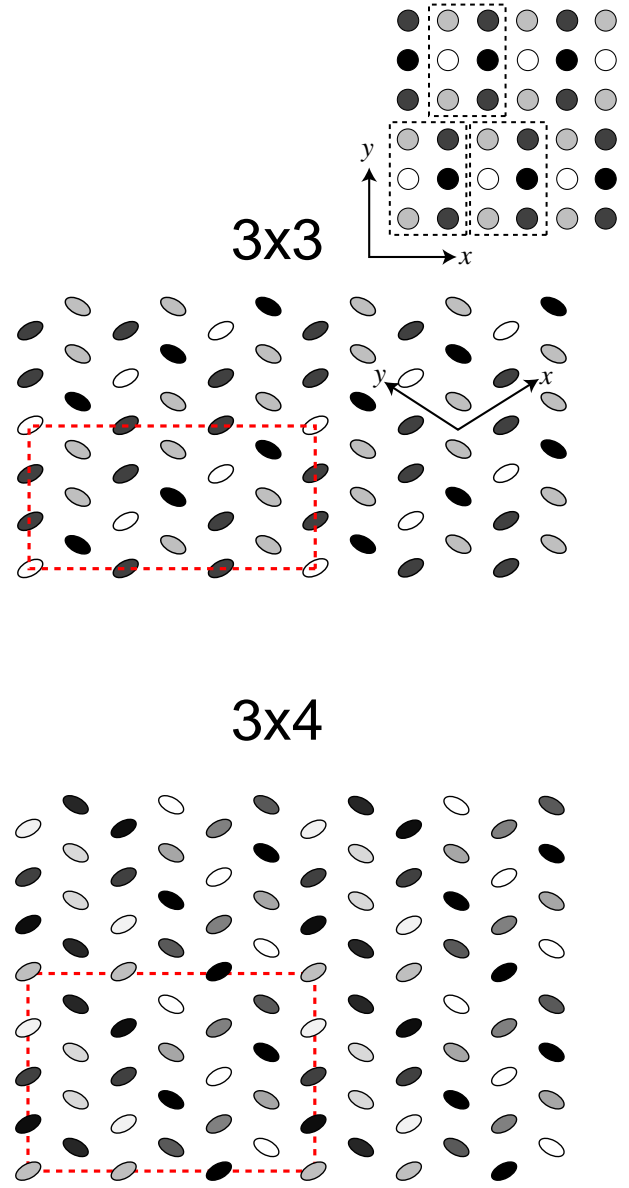


Fig. 12. (Color online) 3×3 and 3×4 charge ordering patterns are shown. The dashed red rectangles represent the unit cell. In the upper inset of the 3×3 ordering, the corresponding pattern on the effective x - y square lattice, for which the actual mean field calculation was done, is displayed along with the unit cell that contains 6 sites.

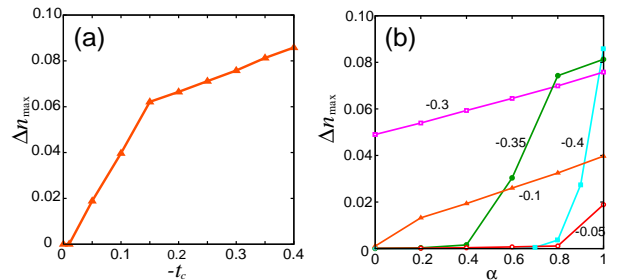


Fig. 13. (Color online) (a) Δn_{max} obtained in the mean field calculation plotted as a function of t_c . (b) Δn_{max} for various choices of t_c plotted as functions of the parameter α that controls the distant (next nearest neighbor) part of the off-site repulsions.

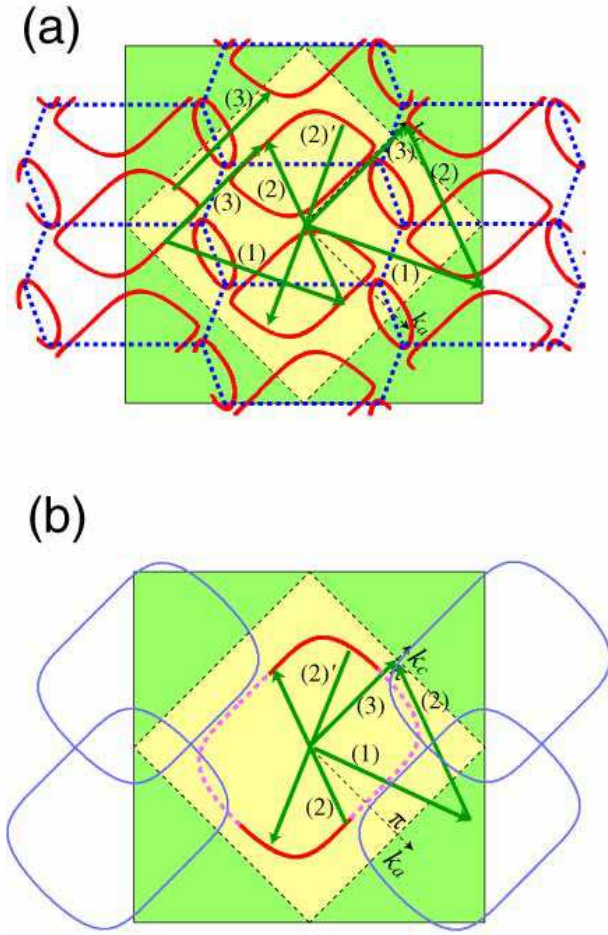


Fig. 14. (Color online) (a) Fermi surface of the 3×3 charge ordered state obtained by the mean field approximation. $U = 5.0$, $V_p = 2.2$, $V_c = 2.5$, $V_a = 0.5$, $V_q = 0.8$, $V_{2c} = 1.2$, and $t_c = -0.3$. The original folded and unfolded BZ are also shown. The dashed lines represent the boundaries of the new BZ. See text for the explanation of the vectors (1)~(3). (b) The expected Fermi surface for the 3×4 charge ordered state (see text).

probably because the nesting vector of the Fermi surface best matches the 3×3 ordering at this particular t_c , but we believe that the 3×3 charge ordering state is not the ground state at least when $\alpha = 0$ considering our RPA results. (Note that we do not compare the total energy between different states as mentioned in section 2.3.)

Now we turn to the Fermi surface in the charge ordered state. In Fig.14(a), we show the Fermi surface in the 3×3 charge ordered state for $t_c = -0.3$ and $\alpha = 1$. Note that the new BZ and the Fermi surface here are “unfolded” in the sense that the unit cell in the inset of Fig.12 neglects the alternation of the molecules in the a -direction. (Therefore, the area of the new BZ is not $1/9$ of the folded BZ but $1/6$ of the unfolded BZ.) We find that some portions of the Fermi surface remain ungapped, so that the system should be metallic, which is consistent with the experiments, where the system remains metallic when diffuse X-ray spots are observed at $(\frac{2}{3}, k, \frac{1}{3} \sim \frac{1}{4})_f$. What is even more interesting is that there is a nesting of the remaining Fermi surface with a nesting vector (3), which is close to $(\frac{1}{4}, \frac{1}{4})_{uf} = (0, \frac{1}{2})_f$, i.e., the modulation vector of the horizontal stripe ordering. This “new

nesting” originates from the fact that there are actually two different nesting vectors in the original system by symmetry, $(+\frac{2}{3}, \frac{1}{3} \sim \frac{1}{4})_f$ and $(-\frac{2}{3}, \frac{1}{3} \sim \frac{1}{4})_f$. The former nesting is used to form the present 3×3 ordering, while the latter nesting (vector (2) and (2)’, where $(2) = (2)′ + (0, 1)_{uf}$) remains in the ordered state,³⁹ although modified to some extent from the original nesting vector because of the deformation of the Fermi surface. In Fig.14(a), vector (1) $= (+\frac{2}{3}, \frac{1}{3})_f$ is a reciprocal lattice vector of the 3×3 ordered state at which a finite Fourier component of the charge density exists, so that the remaining portions of the original Fermi surface translated by vector (1) can interact with one another in the ordered state. Since $(2) + (1) = (3)$ holds, the original nesting at vector (2) results in a “new nesting” of the Fermi surface at vector (3) in the ordered state, which is close to $(0, \frac{1}{2})_f$ especially when the c component of vector (2) (modified due to ordering) is relatively small. Since we know from the RPA results that the charge fluctuations are enhanced in the non-ordered state around vector (2) due to the electron-electron interactions, we may expect that the charge fluctuations are enhanced around the new nesting vector (3) in the 3×3 ordered state due to the electron-electron interactions, although this remains to be confirmed in a future study.⁴⁰

Although our mean field analysis is restricted to the 3×3 charge ordering, we can predict what the Fermi surface should look like in the case of 3×4 ordering from the analogy to the 3×3 case. In Fig.14(b), we show the expected Fermi surface when the 3×4 ordering occurs, where the dashed pink lines are the portions that are expected to vanish due to the $(+\frac{2}{3}, \frac{1}{4})_f$ nesting of the original Fermi surface. The remaining Fermi surface in the 3×4 ordered state is expected to be nested to some extent with the nesting vector close to $(-\frac{2}{3}, \frac{1}{4})_f$ (vectors (2) and (2)’, where $(2) = (2)′ + (0, 1)_{uf}$). In Fig.14(b), $(2) + (1) = (3)$ holds, where vector (1) $= (+\frac{2}{3}, \frac{1}{4})_f$ is a reciprocal lattice vector of the 3×4 ordered state at which a finite Fourier component of the charge density exists. The resulting “new nesting vector” (3) is precisely $(0, \frac{1}{2})_f$ when vector (2) is $(-\frac{2}{3}, \frac{1}{4})_f$. This precise coincidence between the new nesting vector and the horizontal stripe modulation vector comes from the fact that $q_c = \frac{1}{4}$ of both the 3×4 modulation wave vector (1) and the nesting vector (2) is exactly half of $q_c = \frac{1}{2}$ of the horizontal stripe modulation vector.

Now let us recall that within the RPA approach, we could not find any trace of $(0, \frac{1}{2})_f$ charge fluctuations. We propose here a possibility that the new $\sim (0, \frac{1}{2})_f$ Fermi surface nesting in the $3 \times (3 \sim 4)$ charge ordered metallic state triggers, or at least plays some role in, the occurrence of the horizontal (short or long ranged) charge ordering in $X = MM′(\text{SCN})_4$ at low temperatures. In this view, the two charge orderings, the horizontal stripe and $3 \times (3 \sim 4)$, are not independent competing orderings, but the former is “based” on the latter, and therefore we may call the $3 \times (3 \sim 4)$ ordering the “first stage ordering”, and the horizontal stripe ordering the “second stage”. In this sense, the horizontal stripe should be more “fragile” as compared to $3 \times (3 \sim 4)$, which explains why it is the horizontal stripe ordering that is destroyed by

applying the electric field in $X = \text{CsM}'(\text{SCN})_4$.⁴ Also, when the second stage ordering takes place, most of the remaining ungapped Fermi surface in the first stage ordering should disappear, which also explains the (nearly) insulating behavior when the horizontal stripe ordering sets in.

Let us now go back to Fig.11 obtained within RPA. In the present terminology, T_{co} is the temperature where the first stage charge ordering takes place. If the second stage charge ordering is indeed based on the first stage ordering, then we may consider that this t_c dependence of T_{co} should also roughly represent the t_c dependence of the temperature of the second stage ordering at $(0, \frac{1}{2})_f$. In this sense, we may say that Fig.11 is closely related to the experimental phase diagram by Mori et al.² This view is also consistent with an experimental analysis under uniaxial pressure, which concludes that the value of t_c is the key that dominates the occurrence of the horizontal charge ordering.⁴¹

4. Possibility of Superconductivity: an RPA analysis

Having found that the distant off-site interactions are necessary in order to understand the charge orderings and fluctuations of θ -(BEDT-TTF) compounds with $t_c < 0$, we now investigate the possibility of superconductivity induced by such charge fluctuations. Since superconductivity is observed in $X = \text{I}_3$, which has a positive t_c ,⁴²⁻⁴⁴ we concentrate on the case of $t_c > 0$. In fact, the value $t_c/t_p \simeq 0.19$ estimated by Mori for $X = \text{I}_3$,⁴² falls close to a point at which T_{co} falls rapidly in Fig.11, so that a charge fluctuation mediated superconductivity is possible. Here we mainly focus on two sets of off-site interaction values that give the correct charge susceptibility peak positions at $t_c = -0.3$, i.e., $U = 4$, $V_p = 1.8$, $V_c = 2$ with $V_a = 0.4$, $V_q = 0.7$, $V_{2c} = 1.1$ or with $V_a = 0.6$, $V_q = 0.6$, $V_{2c} = 1.1$ (see Fig.10). Using the RPA+gap equation approach, we search for superconductivity within the temperature range of $T > 0.002t_p$ under the condition that the denominator in the charge susceptibility formula (eq.(2)) is larger than 0.02.

First, let us show the results for $V_a = 0.4$, $V_q = 0.7$, $V_{2c} = 1.1$. In this case, we find that the spin singlet pairing dominates over triplet pairing. The obtained spin-singlet gap function is shown in Fig.15 (Δ_{singlet}) along with the Fermi surface. The gap function changes sign as $+ - + -$ along the Fermi surface with nodes intersecting at positions on the k_x and k_y axes as in the d_{xy} pairing. However, the entire gap function roughly has the form

$$\begin{aligned} \Delta(\mathbf{k}) &\propto \cos(k_x - k_y) - 0.8 \cos(k_x + k_y) \\ &+ 0.3[\cos(3k_x + 2k_y) + \cos(2k_x + 3k_y)] \\ &- 0.2[\cos(2k_x - k_y) + \cos(k_x - 2k_y)] \\ &- 0.2 \cos(4k_x + 4k_y), \end{aligned} \quad (10)$$

so that there is a deviation from the simple d_{xy} gap form $\cos(k_x - k_y) - \cos(k_x + k_y) \propto \sin(k_x) \sin(k_y)$. The additional terms such as $\cos(3k_x + 2k_y)$, $\cos(2k_x - k_y)$, and $\cos(4k_x + 4k_y)$ imply that the pairing occurs to some

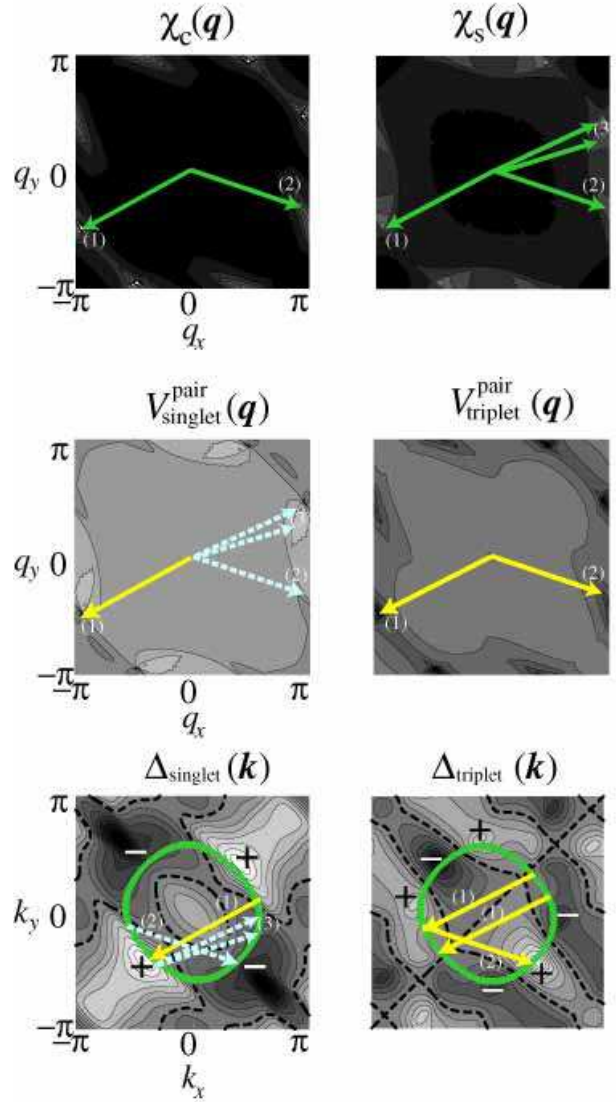


Fig. 15. (Color online) Contour plots of the spin and charge susceptibilities, singlet and triplet pairing interactions, and the singlet (d_{xy} -wave like) and triplet (p_x+2y -wave like) gap functions for $U = 4.0$, $V_p = 1.8$, $V_c = 2.0$, $V_a = 0.4$, $V_q = 0.7$, $V_{2c} = 1.1$, $t_c = 0.14$, and $T = 0.01$. The gap functions are those that give the largest eigenvalue λ for the singlet and triplet pairing channels. The Fermi surface for $t_c = 0.14$ (green solid line) is superposed in the figures of the gap function. The dashed lines in the gap functions represent the nodal lines. Spin and charge fluctuations around wave vectors (1) ~ (3) play important roles in determining the pairing symmetry (see text). The yellow solid (light blue dashed) arrows indicate positive (negative) values of the pairing interactions.

extent at distances $(\Delta x, \Delta y) = \pm(3, 2), \pm(2, -1)$, and $\pm(4, 4)$ (in units of the lattice constants in the x and y directions), respectively, which can be considered as a consequence of the distant off-site repulsions that push away the electrons to far distances.

T_c is plotted as a function of t_c in Fig.16(a), where it is enhanced in the vicinity of the charge ordering phase. For comparison, we also plot T_c in the absence of all the off-site repulsions, where the pairing is solely due to the spin fluctuations, and the charge fluctuations virtually do not contribute. Since T_c is higher in the presence of the off-

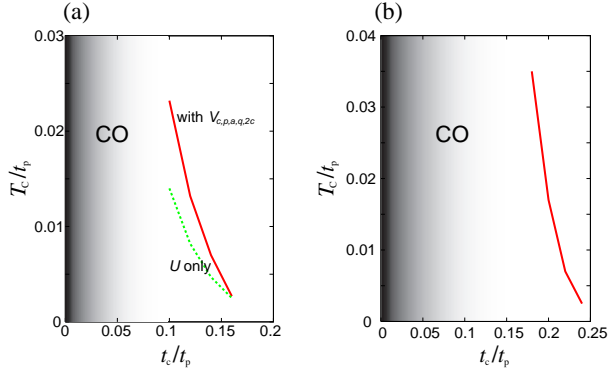


Fig. 16. (Color online) (a) Red solid line : T_c for the singlet d_{xy} -wave pairing as a function of t_c with $U = 4.0$, $V_p = 1.8$, $V_c = 2.0$, $V_a = 0.4$, $V_q = 0.7$, and $V_{2c} = 1.1$. Green dashed line: Same as in the red solid line except all the off-site repulsions are turned off. (b) T_c for the triplet p_x+2y -wave pairing as a function of t_c with $U = 4.0$, $V_p = 1.8$, $V_c = 2.0$, $V_a = 0.6$, $V_q = 0.6$, and $V_{2c} = 1.1$.

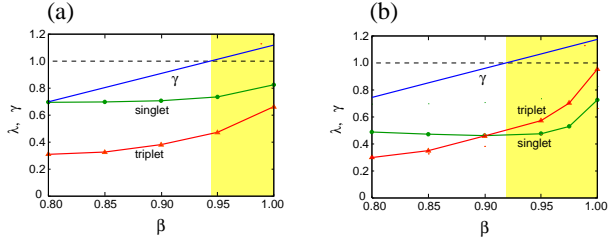


Fig. 17. (Color online) (a) The eigenvalues of the gap equation for the spin singlet and triplet pairings, along with the ratio γ that measures the relative strength ratio between the spin and charge fluctuations (see text), are plotted as functions of β , where the distant interactions are taken as $(V_p, V_c, V_a, V_q, V_{2c}) = \beta(1.8, 2.0, 0.4, 0.7, 1.1)$. $U = 4.0$, $t_c = 0.16$, and $T = 0.02$ are taken. The yellow hatched area is the regime where charge fluctuations dominate over spin fluctuations. (b) Same with (a) except $(V_p, V_c, V_a, V_q, V_{2c}) = \beta(1.8, 2.0, 0.6, 0.6, 1.1)$ and $t_c = 0.2$.

site repulsions while the pairing symmetry is unchanged, we can say that the charge fluctuations cooperate with the spin fluctuations to enhance this superconductivity. This is also seen in Fig.17(a), where we plot the maximum eigenvalue of the gap equation λ for the singlet and the triplet pairings for cases in which all the off-site repulsions $(V_c, V_p, V_a, V_q, V_{2c})$ are multiplied by a factor β ($\beta = 1$ corresponds to $V_c = 2$, $V_p = 1.8$, $V_a = 0.4$, $V_q = 0.7$, $V_{2c} = 1.1$). Here we also plot a ratio γ defined as

$$\gamma = \frac{[-\{U + 2V(\mathbf{q})\}\chi_0(\mathbf{q})]_{\max}}{[U\chi_0(\mathbf{q})]_{\max}}. \quad (11)$$

The denominator and the numerator in this ratio are terms that appear in the denominator of the spin and charge susceptibilities, respectively, and the subscript “max” denotes the maximum value within the entire BZ. Roughly speaking, the charge fluctuations dominate over spin fluctuations (the peak value of the charge susceptibility exceeds that of the spin susceptibility) when γ exceeds unity. We can see from Fig.17(a) that in the charge fluctuation dominating regime, the spin singlet pairing (as well as the triplet pairing) is indeed enhanced as the

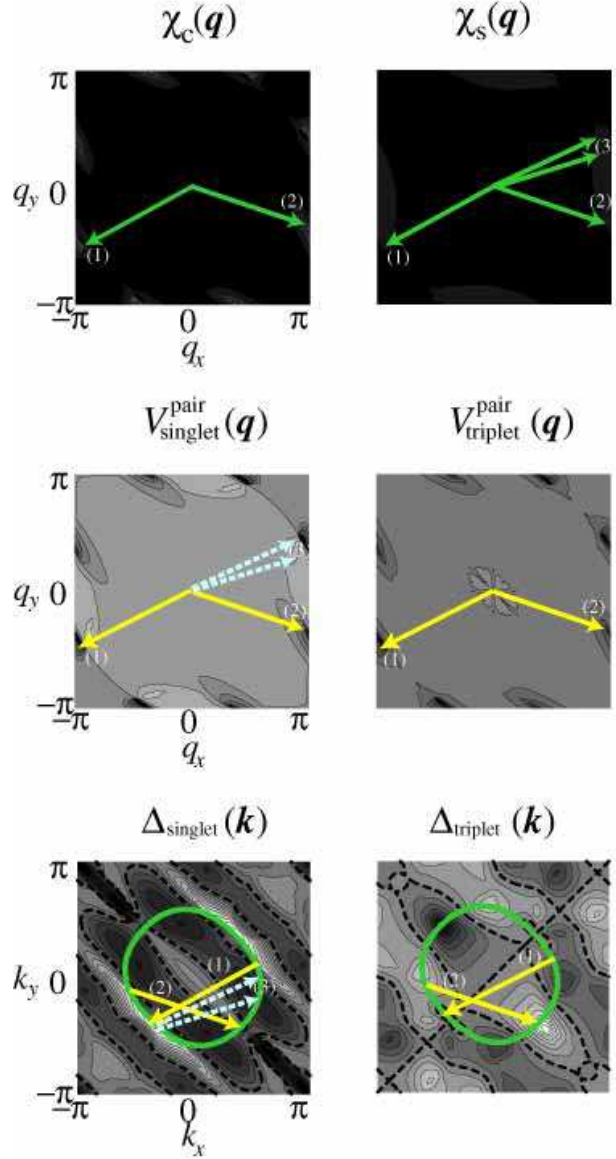


Fig. 18. (Color online) Plots similar to Fig.15 except that $V_a = 0.6$, $V_q = 0.6$, $V_{2c} = 1.1$, and $t_c = 0.2$.

off-site repulsions are increased.

To see this point in more detail, we plot the spin and charge susceptibilities, the singlet and triplet pairing interactions and the gap functions in Fig.15. The spin susceptibility has a peak around wave vector (1), which bridges the portions of the Fermi surface with the same sign of the gap in the singlet d_{xy} pairing, and therefore work destructively against this pairing. (Note that $\Delta(\mathbf{k})\Delta(\mathbf{k}')V^{pair}(\mathbf{k}-\mathbf{k}') < 0$, $\mathbf{k}, \mathbf{k}' \in$ Fermi surface, is favorable for superconductivity with a gap function $\Delta(\mathbf{k})$.) However, the spin susceptibility takes relatively large values also around wave vectors (3)~(2), which bridges the portions of the Fermi surface with different gap signs in the d_{xy} pairing. So the spin fluctuations have components which favor (around (1)) and unfavor (around (2) ~ (3)) the d_{xy} pairing. On the other hand, the charge susceptibility strongly peaks near position (1), very close

to the peak position of the spin susceptibility, at which the spin fluctuations work destructively against the d_{xy} pairing. The charge fluctuation around position (1) is so strong that it cancels out the spin fluctuation contribution (see eq.(6)) and even turns the singlet pairing interaction ($V_{singlet}^{pair}$ in Fig.15) into a negative value at this position, thereby enhancing the d_{xy} pairing.

Now let us turn to the case of $V_a = V_q = 0.6$, $V_{2c} = 1.1$. Although the changes in the parameter values are not so large, and the peak position of the charge susceptibility for $t_c = -0.3$ is very close to that in the case of $V_a = 0.4$, $V_q = 0.7$, $V_{2c} = 1.1$, we find that spin triplet pairing with a gap shown in Fig.18 ($\Delta_{triplet}$) dominates over singlet in this case. T_c of the triplet pairing is shown as a function of t_c in Fig.16(b), where superconductivity is again enhanced in the vicinity of the charge ordering phase. The reason why spin-triplet pairing is enhanced is because the charge fluctuations arise around positions (1) \sim (2) (note that $(\frac{1}{2}, k_y)$ and $(-\frac{1}{2}, k_y)$ are identical points) shown in Fig.18, thus giving rise to attractive triplet pairing interaction around position (2), which favors the gap $\Delta_{triplet}$ because vector (2) bridges the portions of the Fermi surface that have the same gap sign. An analysis similar to the one done for the singlet pairing shows that the gap roughly has the form

$$\begin{aligned} \Delta(\mathbf{k}) &\propto \sin(k_x + 2k_y) - \sin(2k_x + k_y) \\ &- 0.3 \sin(k_x - k_y) + 0.3[\sin(2k_x) - \sin(2k_y)] \\ &- 0.3[\sin(4k_x) - \sin(4k_y)] \\ &+ 0.3[\sin(k_x - 2k_y) - \sin(k_y - 2k_x)]. \quad (12) \end{aligned}$$

The dominating part has the form $\propto \sin(k_x + 2k_y) - \sin(2k_x + k_y)$, so we will call this pairing p_{x+2y} -wave pairing. Although the pairing occurs mainly between sites separated by $\pm(1, 2)$ and $\pm(2, 1)$, here again, the pairs are also formed, to some extent, at far distances. The difference from the case of $V_a = 0.4$, $V_q = 0.7$ is that the charge fluctuations tend to spread out toward position (2) in the case of $V_a = V_q = 0.6$, so that the absolute value of the attractive triplet pairing interaction around position (2) is larger (~ 50 for $V_a = V_q = 0.6$ and ~ 20 for $V_a = 0.4$, $V_q = 0.7$).⁴⁵ In the case of $V_a = 0.4$, $V_q = 0.7$, the charge fluctuations are more localized around position (1), at which the charge fluctuations do not contribute to p_{x+2y} -wave pairing because vector (1) bridges the portion of the Fermi surface at which the nodes of the p_{x+2y} -wave gap exist. This difference of the charge susceptibility between the two cases originates from the structure of $V(\mathbf{q})$ discussed in section 3.1 (note that the value of t_c does not affect $V(\mathbf{q})$), namely, $-V(\mathbf{q})$ is larger around $\mathbf{q} = (\frac{1}{2}, -\frac{1}{6})_{uf} \sim (\frac{11}{24}, -\frac{5}{24})_{uf}$, i.e., position (2), for smaller V_q and larger V_a , so that the charge fluctuations spread out toward position (2) even when $t_c > 0$, although the peak itself is at position (1) for $t_c > 0$ because the nesting vector is now close to that position. As a consequence of the difference in the charge fluctuations, a difference arises also in the spin singlet pairing gap function. Namely, the strong charge fluctuations around position (2) in the case of $V_a = V_q = 0.6$ results in attractive singlet pairing in-

teraction not only near position (1) as in $V_a = 0.4$, $V_q = 0.7$, but also near position (2), which works destructively against d_{xy} pairing, resulting in a vanishing gap around $k_x = -k_y$ (end point of vector (2) in $\Delta_{singlet}$ of Fig.18) in the singlet channel, thereby giving way to spin-triplet pairing. In fact, we can see from Fig.17 that triplet pairing dominates over singlet in the charge fluctuation dominating regime when $(V_a, V_q) = \beta(0.6, 0.6)$ (Fig.17(b)), while singlet pairing continues to dominate deep within the charge fluctuation dominating regime when $(V_a, V_q) = \beta(0.4, 0.7)$ (Fig.17(a)).

So the bottom line here for the superconductivity in the case of $t_c > 0$ is that spin triplet pairing tends to dominate over spin singlet pairing when the off-site interaction values are those that give strong charge fluctuations (namely high T_{co}) for $t_c < 0$ near the position where the diffuse X-ray spots are observed in $X = MM'(SCN)_4$. This tendency is more systematically seen in Fig.10, where we classify the values of (V_a, V_q) at which triplet (singlet) pairing dominates for $t_c = +0.2$ by red (green) circles. Considering the ambiguity in the values of the on-site and off-site repulsions, we cannot predict at the present stage whether singlet or triplet pairings dominate in $X = I_3$. The singlet-triplet competition is subtle, but in any case, the presence of the charge fluctuations enhances superconductivity.

5. Comparison with (TMTSF)₂X

The coexistence of spin and charge fluctuations near the nesting vector " \mathbf{Q}_{2k_F} " of the Fermi surface (although the nesting is not so good for $t_c > 0$) is reminiscent of a quasi-one-dimensional organic superconductor (TMTSF)₂PF₆, in which we have proposed a pairing mechanism due to the coexistence of $2k_F$ spin and $2k_F$ charge fluctuations.²⁹⁻³² In this material, coexistence of $2k_F$ SDW and $2k_F$ CDW has been experimentally observed in the insulating phase sitting next to the superconducting phase in the pressure-temperature phase diagram.^{46, 47} This coexistence cannot be understood within a model that considers only the on-site U and the nearest neighbor repulsion V , and the effect of the second nearest neighbor repulsion V' is crucial,^{27-29, 31, 33, 34} sharing similarity with the present case. In fact, the mechanism of $2k_F (= \frac{\pi}{4} \times 2 = \frac{\pi}{2})$ CDW in TMTSF is very similar to the mechanism of $3 \times (3 \sim 4)$ ordering proposed in the present study. Namely, if we consider only the nearest (V) and the next nearest neighbor (V') interactions within the chains, the Fourier transform of the off-site repulsions is given as $V(\mathbf{q}) = 2V \cos(q_x) + 2V' \cos(2q_x)$. On the other hand, the bare susceptibility $\chi_0(\mathbf{q})$ has a peak at $q_x = \frac{\pi}{4}$ due to a good nesting of the Fermi surface of the quarter-filled quasi-1D band. Since both $-V(\mathbf{q})$ and $\chi_0(\mathbf{q})$ take large positive values at $q_x = \frac{\pi}{2}$, $2V(\mathbf{q})\chi_0(\mathbf{q})$ in the denominator of eq.(2) takes a large negative value there, resulting in a peak in the charge susceptibility at $2k_F$. Therefore, within this scenario, the $2k_F$ CDW in (TMTSF)₂PF₆ occurs precisely due to a cooperation between the effect of the off-site (next nearest neighbor) repulsions and the Fermi surface nesting.

In the case of (TMTSF)₂PF₆, due to the good nesting of the Fermi surface and the one dimensionality, the

$2k_F$ peak positions as well as the overall \mathbf{q} dependence of the spin and charge susceptibilities nearly coincide, so that the two fluctuations work destructively in the singlet pairing (eq.(6)) while constructively in the triplet pairing (eq.(7)). Also, due to the quasi-one-dimensionality of the system, the Fermi surface is disconnected in a manner that spin singlet d -wave-like pairing and spin-triplet f -wave-like pairing have the same number of nodes on the Fermi surface.³⁰ Due to these factors favoring spin triplet pairing, charge fluctuations with similar strength with the spin fluctuation result in a subtle competition between f -wave and d -wave pairings in a realistic parameter regime.^{31, 32, 34}

In the present case of the θ -(BEDT-TTF) compounds, there are several differences as compared to TMTSF: (i) there is a large component in the spin fluctuations that work destructively against singlet pairing, (ii) the charge fluctuations cancel out this spin fluctuation component in the singlet pairing interaction to enhance the pairing, (iii) The singlet pairing has smaller number of nodes on the Fermi surface than in the triplet pairing because there is no disconnectivity in the Fermi surface. (iv) since there are 6 nearest neighbor (V_p , V_c) and 8 next nearest neighbor (V_a , V_q , V_{2c}) interactions in the θ compounds as compared to 4 nearest (including the interchain direction) and 2 next nearest neighbor interactions in (TMTSF)₂X, $V(\mathbf{q})$ tends to be large, so that the charge fluctuations are likely to strongly dominate over spin fluctuations in a realistic parameter regime. In the charge fluctuation dominating regime, the charge fluctuations enhance both singlet and triplet pairings, but the enhancement in the latter is stronger. Factors (i) and (iv) favor triplet pairing, while (ii) and (iii) singlet pairing. Due to these competing factors, there is a close competition between singlet and triplet pairing once again as in (TMTSF)₂X.

6. Conclusion

In the present study, we have investigated the origin of the charge orderings in θ -(BEDT-TTF)₂MM'(SCN)₄. We have shown that neither the low temperature horizontal stripe nor the high temperature $3 \times (3 \sim 4)$ charge orderings can be understood within a model that takes into account only U , V_p , and V_c as electron-electron repulsions. We have shown that the $3 \times (3 \sim 4)$ charge ordering can be considered as a consequence of the cooperation between the effect of the off-site repulsions including the distant interactions V_a , V_q , and V_{2c} , and the nesting of the Fermi surface. Moreover, we have proposed a possibility that the horizontal stripe charge ordering is triggered by the new $(0, \frac{1}{2})_f$ nesting in the $3 \times (3 \sim 4)$ charge-ordered state, where some portions of the Fermi surface remain ungapped. From this viewpoint, we can understand why the horizontal stripe charge ordering temperature decreases with increasing t_c (from $t_c < 0$ to $t_c > 0$) in θ -(BEDT-TTF)₂X. Namely, as t_c increases, the nesting of the Fermi surface is degraded, the maximum positions of $\chi_0(\mathbf{q})$ and $-V(\mathbf{q})$ deviate, and the density of states becomes small, all working destructively against $3 \times (3 \sim 4)$ ordering. Since $3 \times (3 \sim 4)$ "first stage" ordering gives base for the horizontal stripe "second stage"

ordering in our view, the temperature of the latter ordering should also become low as t_c increases.

In the present study, we have obtained the Fermi surface of the 3×3 charge ordered state by assuming that this first stage ordering is truly long ranged, while it is not a true long range order in the actual materials. Also, the role of the electron-electron interactions in the occurrence of the second stage ordering as well as the second stage ordering temperature has not been addressed quantitatively. A more detailed and quantitative understanding of this "successive charge ordering" view, as well as the investigation on its possible relevance to the nonlinear transport,^{3, 4} serves as an interesting future study.

Given that the distant interactions are important in θ -(BEDT-TTF)₂X, we have further investigated the possibility of superconductivity in the vicinity of the charge ordering phase for $t_c > 0$. We have shown that there is a close competition between d_{xy} -wave-like singlet pairing and p_{x+2y} -wave-like triplet pairing, where the latter tends to dominate over the former when we adopt the interaction values that give strong charge fluctuations (high T_{co}) around $(\frac{2}{3}, \frac{1}{3} \sim \frac{1}{4})_f$ in the case of $t_c < 0$. Regardless of whether triplet pairing dominates or not, the charge fluctuations are found to enhance superconductivity.

In total, we have provided a unified understanding of the overall phase diagram of θ -(BEDT-TTF)₂X² at least qualitatively within an electronic model that considers the band structure and the electron-electron interactions up to next nearest neighbors.

Acknowledgement

The author would like to thank H. Mori, T. Mori, T. Yamaguchi, H. Seo, and R. Arita for discussions. The author acknowledges Grants-in-Aid for Scientific Research from the Ministry of Education, Culture, Sports, Science and Technology of Japan, and from the Japan Society for the Promotion of Science. Part of the numerical calculation has been performed at the facilities of the Supercomputer Center, Institute for Solid State Physics, University of Tokyo.

- 1) H. Mori, S. Tanaka, T. Mori, and Y. Maruyama: Bull. Chem. Soc. Jpn. **68** (1995) 1136.
- 2) H. Mori, S. Tanaka, and T. Mori: Phys. Rev. B **57** (1998) 12023.
- 3) K. Inagaki, I. Terasaki, H. Mori, and T. Mori: J. Phys. Soc. Jpn. **73** (2004) 3364.
- 4) F. Sawano, I. Terasaki, H. Mori, T. Mori, M. Watanabe, N. Ikeda, Y. Nogami, and Y. Noda : Nature **437** (2005) 522.
- 5) Y. Nogami, J.-P. Pouget, M. Watanabe, K. Oshima, H. Mori, S. Tanaka, and T. Mori : Synth. Met. **103** (1999) 1911.
- 6) M. Watanabe, Y. Nogami, K. Oshima, H. Mori, and S. Tanaka : J. Phys. Soc. Jpn. **68** (1999) 2654.
- 7) M. Watanabe, Y. Noda, Y. Nogami, and H. Mori : J. Phys. Soc. Jpn. **73** (2004) 116.
- 8) M. Watanabe, Y. Noda, Y. Nogami, and H. Mori : J. Phys. Soc. Jpn. **74** (2005) 2011.
- 9) K. Miyagawa, A. Kawamoto, and K. Kanoda : Phys. Rev. B **62** (2000) R7679.
- 10) R. Chiba, H. Yamamoto, K. Hiraki, T. Takahashi, and T. Nakamura : J. Phys. Chem. Solids **62** (2001) 389.
- 11) H. Seo: J. Phys. Soc. Jpn. **69** (2000) 805.

- 12) H. Mori, S. Tanaka, T. Mori, A. Kobayashi, and H. Kobayashi : Bull. Chem. Soc. Jpn. **71** (1998) 797.
- 13) H. Tajima, S. Kyoda, H. Mori, and S. Tanaka : Synth. Met. **120** (2001) 757.
- 14) K. Yamamoto, K. Yakushi, K. Miyagawa, K. Kanoda, and A. Kawamoto : Phys. Rev. B **65** (2002) 85110.
- 15) R.H. McKenzie, J. Merino, J.B. Marston, and O.P. Sushkov : Phys. Rev. B **64** (2001) 085109.
- 16) K. Hanasaki and M. Imada : J. Phys. Soc. Jpn. **74** (2005) 2769.
- 17) T. Mori : J. Phys. Soc. Jpn. **72** (2003) 1469.
- 18) R.T. Clay, S. Mazumdar, D.K. Campbell: J. Phys. Soc. Jpn. **71** (2002) 1816.
- 19) J. Merino, H. Seo, and M. Ogata: Phys. Rev. B **71** (2005) 125111.
- 20) M. Kaneko and M. Ogata: J. Phys. Soc. Jpn. **75** (2006) 014710.
- 21) H. Watanabe and M. Ogata: J. Phys. Soc. Jpn. **75** (2006) 063702.
- 22) C. Hotta, N. Furukawa, A. Nakagawa, and K. Kubo : cond-mat/0607717.
- 23) H. Kobayashi, R. Kato, A. Kobayashi, Y. Nishio, K. Kajita, and W. Sasaki : Chem. Lett. (1986) 789.
- 24) J. Merino and R.H. McKenzie : Phys. Rev. Lett. **87** (2001) 237002.
- 25) A. Kobayashi, Y. Tanaka, M. Ogata, and Y. Suzumura : J. Phys. Soc. Jpn. **73** (2004) 1115.
- 26) Y. Takahide, T. Konoike, K. Enomoto, M. Nishimura, T. Terashima, S. Uji, and H.M. Yamamoto: Phys. Rev. Lett. **96** (2006) 136602.
- 27) N. Kobayashi and M. Ogata: J. Phys. Soc. Jpn. **66** (1997) 3356; N. Kobayashi, M. Ogata and K. Yonemitsu: J. Phys. Soc. Jpn. **67** (1998) 1098.
- 28) Y. Tomio and Y. Suzumura: J. Phys. Soc. Jpn. **69** (2000) 796.
- 29) Y. Tanaka and K. Kuroki, Phys. Rev. B, **70** (2004) 060502.
- 30) K. Kuroki, R. Arita, and H. Aoki: Phys. Rev. B **63** (2001) 094509.
- 31) K. Kuroki and Y. Tanaka : J. Phys. Soc. Jpn. **74** (2005) 1694.
- 32) K. Kuroki : J. Phys. Soc. Jpn. **75** (2006) 051013.
- 33) Y. Fuseya and Y. Suzumura : J. Phys. Soc. Jpn. **74** (2005) 1263.
- 34) J.C. Nickel, R. Duprat, C. Bourbonnais, and N. Dupuis : Phys. Rev. Lett. **95** (2005) 247001.
- 35) D. J. Scalapino, E. Loh, and J. E. Hirsch: Phys. Rev. B **35** (1987) 6694.
- 36) Y. Tanaka, Y. Yanase and M. Ogata: J. Phys. Soc. Jpn. **73** (2004) 319.
- 37) The decrease of the density of states with the increase of t_c has also been pointed out in C.Hotta: J. Phys. Soc. Jpn. **72** (2003) 840.
- 38) The reason we chose values of interactions to be slightly larger than that in the RPA calculation is because Δn_{\max} , if any, becomes very small if we adopt the values used in the RPA. This is probably because we assume no ordering in the spin density in the present mean field calculation, whereas in the RPA calculation, the spin susceptibility does have a well defined peak at the nesting vector.
- 39) Due to symmetry, the opposite can also happen with the same probability, i.e., the 3×3 ordering using the $(-\frac{2}{3}, \frac{1}{3} \sim \frac{1}{4})_f$ nesting, resulting in a new nesting near $(0, \frac{1}{2})_f$ due to the original $(+\frac{2}{3}, \frac{1}{3} \sim \frac{1}{4})_f$ nesting. There is also a possibility that the two charge orderings with different modulation simultaneously set in at the same temperature, resulting in a state with an almost fully gapped Fermi surface. Although in a strict sense this possibility has to be addressed theoretically, such a possibility is unlikely from an experimental point of view considering that the system remains metallic and no X-ray spot is observed at $(0, \frac{1}{2})_f$ in the $3 \times (3 \sim 4)$ ordering state at high temperatures.
- 40) If the a component of vector (2) deviates from $k_a = -\frac{2}{3}$, the a component of vector (3) deviates from $k_a = 0$. In that case, if we consider the ‘‘opposite case’’ mentioned in comment 39, the new nesting vector appears at a position symmetric with respect to the k_c axis. In the actual experiments, the mixture of these two opposite cases should be observed.
- 41) R. Kondo, M. Higa, S. Kagoshima, H. Hoshino, T. Mori, and H. Mori : J. Phys. Soc. Jpn. **75** (2006) 044716.
- 42) H. Mori : private communications.
- 43) H. Kobayashi, R. Kato, A. Kobayashi, Y. Nishio, K. Kajita, and W. Sasaki: Chem. Lett. (1986) 833.
- 44) M. Tamura, K. Yakushi, H. Kuroda, A. Kobayashi, R. Kato, and H. Kobayashi : J. Phys. Soc. Jpn. **57** (1988) 3239.
- 45) To be more precise, the peak absolute value of the triplet pairing interaction at position (1) itself is also larger for $V_a = V_q = 0.6$ and $t_c = 0.2$ (~ 90) than for $V_a = 0.4, V_q = 0.7$ and $t_c = 0.14$ (~ 50). However, if we take $t_c = 0.12$ for $V_a = 0.4, V_q = 0.7$, the peak absolute value at position (1) (~ 160) by far exceeds that for $V_a = V_q = 0.6$ and $t_c = 0.2$, but still the absolute value at position (2) remains to be ~ 20 , meaning that the peak structure is strongly localized.
- 46) J. P. Pouget and S. Ravy: J. Phys. I **6** (1996) 1501.
- 47) S. Kagoshima, Y. Saso, M. Maesato, R. Kondo, and T. Hasegawa : Solid State Comm. **110** (1999) 479.